

MAXI J1957+032: a new accreting millisecond X-ray pulsar in an ultra-compact binary

A. Sanna¹, P. Bult^{2,3}, M. Ng⁴, P. S. Ray⁵, G. K. Jaisawal⁶, L. Burderi¹, T. Di Salvo⁷,
A. Riggio^{1,8}, D. Altamirano⁹, T. E. Strohmayer³, A. Manca¹, K. C. Gendreau³, D. Chakrabarty⁴,
W. Iwakiri¹⁰ and R. Iaria⁷

¹Dipartimento di Fisica, Università degli Studi di Cagliari, SP Monserrato-Sestu km 0.7, 09042 Monserrato, Italy

²Department of Astronomy, University of Maryland, College Park, MD 20742, USA

³Astrophysics Science Division, NASA Goddard Space Flight Center, Greenbelt, MD 20771, USA

⁴MIT Kavli Institute for Astrophysics and Space Research, Massachusetts Institute of Technology, Cambridge, MA 02139, USA

⁵Space Science Division, Naval Research Laboratory, Washington, DC 20375-5352, USA

⁶National Space Institute, Technical University of Denmark, Elektrovej 327-328, 2800 Lyngby, Denmark

⁷Università degli Studi di Palermo, Dipartimento di Fisica e Chimica, via Archirafi 36, 90123 Palermo, Italy

⁸INAF/IASF Palermo, via Ugo La Malfa 153, I-90146 - Palermo, Italy

⁹School of Physics and Astronomy, University of Southampton, Southampton, Hampshire SO17 1BJ, UK

¹⁰Department of Physics, Faculty of Science and Engineering, Chuo University, 1-13-27 Kasuga, Bunkyo-ku, Tokyo 112-8551, Japan

Accepted 2022 August 11. Received 2022 August 5; in original form 2022 July 15

ABSTRACT

The detection of coherent X-ray pulsations at ~ 314 Hz (3.2 ms) classifies MAXI J1957+032 as a fast-rotating, accreting neutron star. We present the temporal and spectral analysis performed using NICER observations collected during the latest outburst of the source. Doppler modulation of the X-ray pulsation revealed the ultra-compact nature of the binary system characterized by an orbital period of ~ 1 h and a projected semimajor axis of 14 lt-ms. The neutron star binary mass function suggests a minimum donor mass of $1.7 \times 10^{-2} M_{\odot}$, assuming a neutron star mass of $1.4 M_{\odot}$ and a binary inclination angle lower than 60 deg. This assumption is supported by the lack of eclipses or dips in the X-ray light curve of the source. We characterized the 0.5–10 keV energy spectrum of the source in outburst as the superposition of a relatively cold black-body-like thermal emission compatible with the emission from the neutron star surface and a Comptonization component with photon index consistent with a typical hard state. We did not find evidence for iron $K\alpha$ lines or reflection components.

Key words: accretion, accretion discs – binaries:general – stars:neutron – X-rays:binaries.

1 INTRODUCTION

Accreting millisecond X-ray pulsars (AMXPs) are rapidly rotating (spin frequency > 30 Hz) neutron stars (NS) gravitationally bound with late-type companion stars (see e.g. Di Salvo & Sanna 2020; Patruno & Watts 2021, for extensive reviews). Their distinct short spin periods are a direct consequence of prolonged mass transfer phases in which the companion star loses matter via Roche lobe overflow, subsequently accreted on to the NS (*recycling scenario*; Alpar et al. 1982). The sample currently includes 24 sources, a third of which are characterized by an orbital period shorter than 80 min (also known as *ultra-compact* binaries). Short orbital periods suggest small low-mass companion stars, consistent with donor masses on average $< 0.2 M_{\odot}$.

MAXI J1957+032 was observed for the first time by MAXI (Negoro et al. 2015) and INTEGRAL (Cherepashchuk et al. 2015) in 2015 May. At odds with standard low-mass X-ray binaries (LMXBs) MAXI J1957+032 exhibited four short (< 5 d) faint outbursts be-

tween its discovery and 2016 October (Sugimoto et al. 2015; Tanaka et al. 2016). Optical observations of the system during its 2016 outburst revealed emission compatible with an irradiated X-ray disc in a LMXB, suggesting similarities with AMXPs (Mata Sánchez et al. 2017). An optical counterpart (late-K/early M dwarf star) has been identified during the X-ray quiescence phase, setting a constraint on the source distance of the order of 5 ± 2 kpc (Ravi 2017). However, the outburst properties of MAXI J1957+032 let the author suggest that the observed counterpart is likely not the mass donor. Instead, it is suggested to be a possible triple system, with the main-sequence counterpart likely being in a wide orbit around a compact interacting binary. Moreover, the spectral evolution investigated by combining the *Swift* observations collected during the four outbursts suggested that, for a distance of the order of 4 kpc, an NS might be hosted in the binary system (Beri et al. 2019).

On June 18, 2022, MAXI/GSC detected X-ray activity in the direction of MAXI J1957+032 (Negoro et al. 2022). NICER quickly started monitoring the new outburst, discovering coherent X-ray pulsations at ~ 314 Hz and revealing the nature of the accreting compact object (Ng et al. 2022). A preliminary orbital solution obtained from continued NICER observations suggests that MAXI J1957+032 is

* E-mail: andrea.sanna@dsf.unica.it

an *ultra-compact* binary with an orbital period of ~ 1 h (Bult et al. 2022).

Swift/XRT observations on 2022 June 20, suggested spectral properties consistent with the 2016 outburst of the source (see e.g. Beri et al. 2019). Moreover, *Swift*/UVOT detected the UV counterpart of the source, with a magnitude $UVW2 = 20.37 \pm 0.08$ (Beri et al. 2022). On June 21, MAXI J1957+032 was not detected in radio by the MeerKAT observatory, with an upper limit of $48 \mu\text{Jy}$ (van den Eijnden et al. 2022). Optical observations suggested the presence of short time-scale variability during the outburst (Baglio et al. 2022), and a significant optical counterpart during the 50 d before the outburst, with the first optical brightening almost 9 h earlier to the MAXI/GSC trigger (Wang, Bellm & Jaodand 2022). On June 23, *Swift* revealed no significant X-ray activity at the source location, suggesting that MAXI J1957+032 may have entered the quiescence phase (Chandra 2022).

Here, we report on the discovery of millisecond X-ray pulsations from the X-ray transient MAXI J1957+032 and its spectral properties from the NICER observations collected during its latest outburst.

2 OBSERVATIONS AND DATA REDUCTION

MAXI J1957+032 was observed by *NICER X-ray telescope* on the *International Space Station* (Gendreau et al. 2016) from 2022 June 19 to June 24 (ObsIDs 5202840101–6) for a total exposure time of ~ 22.5 ks after standard filtering. We also included a short data segment (~ 40 s at MJD ~ 59740.1) collected during a raster scan performed to better constrain the source position. We retained events in the 0.5–10 keV energy band by processing the observations with HEASOFT version 6.30.1 and the *NICER* software *NICERDAS* version 9.0 (2022-01-17_V009) with standard screening criteria. We extracted source and background spectra in the 0.5–10 keV energy range using the *NIBACKGEN3C50* tool (Remillard et al. 2022), and we generated response matrices using the *NICERRMF* and *NICERARF* tools. The analysis was performed with *XSPEC* 12.12.1 (Arnaud 1996) after applying an optimal binning, which guarantees at least 25 counts per energy bin.

The top panel of Fig. 1 shows the background-subtracted light curve of the outburst monitored by *NICER* (black points). Each point represents the 16 s average count rate. ObsIDs 5202840105–6 are not shown since the source count rate is compatible with the background. The source count rate at the peak of the observed outburst is ~ 160 cts s^{-1} , which exponentially decreases to the quiescence level in almost 4 d. No Type-I thermonuclear X-ray bursts were observed during the observations. Finally, we applied barycentric corrections to the photon arrival times utilizing the *BARYCORR* tool adopting JPL DE-405 Solar system ephemeris. We considered the best available source position coordinates obtained by *Chandra* during the 2015 and 2016 outbursts (Chakrabarty, Jonker & Markwardt 2016).

3 RESULTS

3.1 Timing analysis

Following the detection of X-ray pulsations at ~ 314 Hz (Ng et al. 2022), we proceeded by searching for X-ray pulsations over short time intervals (between 150 and 500 s, depending on the statistics of the data segment) by performing epoch-folding search techniques using 8 phase bins and starting with the spin frequency value $\bar{\nu} = 313.643740$ Hz (Bult et al. 2022). We explored the frequency space with a 10^{-5} Hz frequency step for a total of 10001 steps. We detected significant X-ray pulsations in 38 of the 60 data

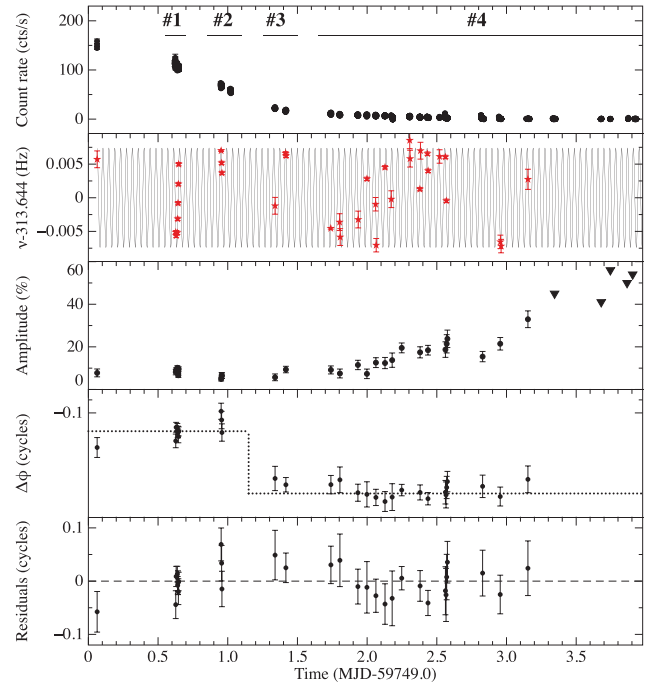


Figure 1. First panel - *NICER* 0.5–10 keV light curve of the 2022 June outburst of MAXI J1957+032. Filled circles represent 16 s average background-subtracted count rate of the source. Second panel - Temporal evolution of the pulsar frequency (with respect to $\nu = 313.644$ Hz) estimated from *NICER* data segments. The solid black line represents the best-fitting orbital Doppler modulation assuming a circular orbit. Third panel - Evolution of the fractional pulse amplitude estimated in the energy range 0.5–10 keV (filled circles), and upper limits (3σ c.l.) on the non-detection (filled triangles). Fourth panel - Evolution of the pulse phase delays obtained by epoch-folding the *NICER* photon arrival times corrected for the best-fitting orbital solution from the phase-coherent analysis. The dotted line serves the purpose of highlighting the phase jump observed around 59750.2 MJD. Fifth panel - Residuals in pulse cycles with respect to the best-fitting models for the pulse phase delays.

segments. The signal frequency value and uncertainty for each data segment have been determined following the method described by Leahy (1987). The temporal evolution of the detected signal (second panel of Fig. 1, red stars) is compatible with an orbital modulation. Assuming a circular orbit, we obtained the best-fit for an orbital period of $P_{\text{orb}} = 3653.47(69)$ s, a projected semimajor axis of the NS orbit $x = 0.01367(35)$ lt-s, an epoch of ascending node passage $T_{\text{ASC}} = 59749.63327(22)$ MJD, and a spin frequency $\bar{\nu} = 313.64373(12)$ Hz (Fig. 1, second panel, solid line).

We then proceeded with the phase-coherent timing analysis by generating pulse phase delays in the time interval between MJD 59749.625494 and MJD 59749.648643 (June 19; for an exposure time of ~ 1.3 ks), where the *NICER* count rate is higher. We folded data segments of ~ 200 s into 8 phase bins at the preliminary spin frequency $\bar{\nu}$. We then modelled each pulse profile with a constant plus a sinusoidal function, and we retained profiles for which the pulse amplitude is at least three times larger than its uncertainty. We modelled the pulse phase evolution with a constant frequency combined with a circular Keplerian orbital model (see Sanna et al. 2016, for a more detailed description of the procedure).

Due to the short baseline covered by the data set with respect to the orbital modulation of the system and the relatively small uncertainties on the orbital period and projected semimajor axes, we only explored corrections on the spin frequency and the epoch of ascending node

Table 1. Orbital parameters and spin frequency of MAXI J1957+032 with uncertainties on the last digit quoted at 1σ confidence level. T_0 represents the reference epoch for this timing solution.

Parameters	
RA (J2000)	$19^{\text{h}}56^{\text{m}}39.11^{\text{s}} \pm 0.04^{\text{s}}$
Dec. (J2000)	$03^{\circ}26'43.7'' \pm 0.6''$
P_{orb} (s)	3653.046(61)
x (lt-s)	0.013796(25)
T_{ASC} (MJD/TDB)	59749.633146(18)
Eccentricity	$< 1.4 \times 10^{-2}$ (3σ c.l.)
ν_0 (Hz)	313.64374049(22)
T_0 (MJD/TDB)	59749.0
$\chi_{\text{red}}^2/\text{d.o.f}$	1.23/23

passage. The best-fit is obtained for $\bar{\nu} = 313.6436542(61)$ Hz, and $T_{\text{ASC}} = 59749.633066(17)$ MJD. We then propagated the solution to the nearest (in time) data segments verifying that the phase uncertainty remained smaller than half of a spin cycle, a condition required for the application of phase-coherent analysis. It is noteworthy that a similar conclusion can be reached even accounting for spin frequency derivatives $|\dot{\nu}| \leq 10^{-11}$ Hz s $^{-1}$, orders of magnitude larger than the values observed for AMXPs (see e.g. Di Salvo & Sanna 2020). We generated pulse phase delays for each increased data set and fitted them, searching for a stable timing solution, until we covered the whole outburst.

As shown in the fourth panel of Fig. 1, the pulse phase delays from the most accurate timing solution show a phase jump of ~ 0.2 pulse cycles around MJD 59750.2. To account for that, we included in the model a phase jump around MJD 59750.2. The best-fitting orbital and pulsar spin parameters from the latter model are reported in Table 1, while its associated residuals are shown in the fifth panel of Fig. 1. A close inspection suggests a further modulation of the residuals on time-scales longer than the binary orbital period. We tested this hypothesis by comparing a constant against a constant plus a sinusoidal function. The latter showed an F-test probability of $\sim 1.7 \times 10^{-3}$, corresponding to a $\sim 3\sigma$ statistical improvement due to the additional component characterized by an amplitude of $(3.3 \pm 0.8) \times 10^{-2}$ phase cycles, and period 1.99 ± 0.14 d.

To further investigate the effect of the phase jump, we generated the average pulse profile pre- and post-phase jump (Fig. 2). Both profiles are well described as the superposition of three harmonically related sinusoidal functions. The fundamental, second, and third harmonics of the pre-jump profile are characterized by fractional amplitudes of (7.9 ± 0.2) per cent, (2.7 ± 0.2) per cent, and (2.0 ± 0.3) per cent, respectively. The post-jump profile presents fractional amplitudes of (10.6 ± 0.4) per cent, (2.9 ± 0.5) per cent, and (0.9 ± 0.4) per cent for the fundamental, second, and third harmonics, respectively.

In the third panel of Fig. 1, we report the evolution of the background-corrected fractional amplitude of the pulse profile estimated from the best-fitting solution (filled circles), as well as upper limits for non-detection (filled triangles). The fractional amplitude remains almost constant around the value of 7.5 per cent for the first 2 d when it starts to increase, reaching a value of ~ 32 per cent during the last signal detection.

3.2 Spectral analysis

We investigated the spectral properties of MAXI J1957+032 by generating four energy spectra along the decaying phase of the outburst. Data intervals selected to create the spectra are shown in Fig. 1. To perform the spectral analysis, we set Wilms, Allen &

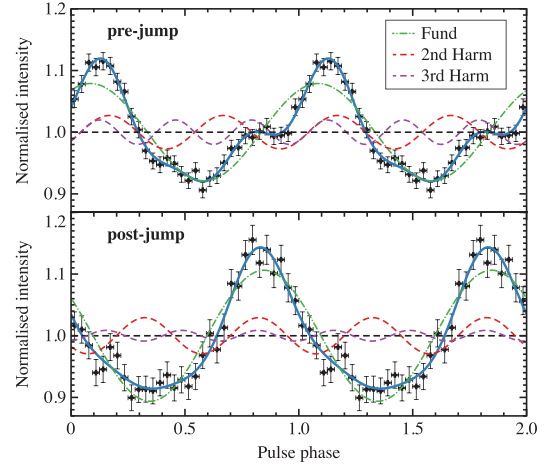


Figure 2. Average pulse profiles (black points) generated combining the NICER data pre- (top-panel) and post- (bottom-panel) appearance of the pulse phase jump (MJD 59750.2) after correcting for the best-fitting orbital parameters reported in Table 1. The best-fitting model (cyan solid line) is well described by the superposition of three harmonically related sinusoidal functions. Two cycles of the pulse profile are shown for clarity.

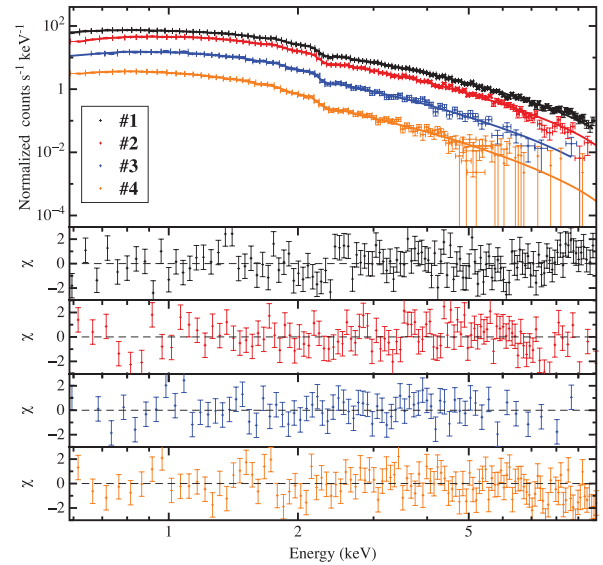


Figure 3. Upper panel: NICER spectra of MAXI J1957+032 obtained by selecting four intervals (#1–#4) during the descending phase of its latest outburst. Black, red, blue, and orange represent intervals #1, #2, #3, and #4, respectively. Solid lines show the best-fitting model to the data. Lower panels: residuals with respect to the best-fitting models expressed in units of standard deviations for each of the spectra analysed.

McCray (2000) elemental abundances and Verner et al. (1996) photo-electric cross-sections. The 0.5–10 keV energy spectra are well modelled by an absorbed thermal component (black-body) combined with a power-law continuum (TBabs*[bbodyrad + power law] in XSPEC).

The best-fitting values of N_{H} vary from $(0.9 \pm 0.1) \times 10^{21}$ cm $^{-2}$ (obtained in #1) up to an average value of $(2.5 \pm 0.5) \times 10^{21}$ cm $^{-2}$ for the other intervals. We noticed that the Galactic absorption in the direction of the source is estimated to be $\sim 1 \times 10^{22}$ cm $^{-2}$ (HI4PI Collaboration et al. 2016). Moving from #1 to #4, the black-body temperature (kT_{BB}) decreased significantly from (0.45 ± 0.01) keV

down to (0.26 ± 0.03) keV, as well as its normalization that varies from (5.3 ± 2.2) km to 1.6_{-1}^{+2} km (estimated at 5 ± 2 kpc; Ravi 2017), compatible with a fraction of the NS surface. The power-law photon index at the peak is $\Gamma = 1.58 \pm 0.04$, compatible with the source being in a hard state. As expected, during the descending phase, Γ increases, reaching the final value of 2.81 ± 0.03 . We detected clear correlations between N_H , kT_{BB} , and Γ by Goodman–Weare algorithm of Monte Carlo Markov Chain (Goodman & Weare 2010) characterized by 20 walkers and chain length of 10^6 . However, the observed spectral evolution cannot be explained only by model degeneracy. We found no evidence for spectral lines (e.g. iron $K\alpha$) nor reflection features. Fig. 3 shows the spectra and residuals with respect to the best-fit model for the four time intervals analysed. Finally, the unabsorbed 0.5–10 keV flux decreases from $(2.95 \pm 0.02) \times 10^{-10}$ erg cm $^{-2}$ s $^{-1}$ to $(8.06 \pm 0.08) \times 10^{-12}$ erg cm $^{-2}$ s $^{-1}$ close to the quiescence phase.

4 DISCUSSION

We reported on the temporal and spectral properties of the newly discovered AMXP MAXI J1957+032 during its latest outburst as monitored by NICER. The detection of coherent X-ray pulsations at ~ 314 Hz allowed us to identify the accreting compact object as a rapidly rotating NS, confirming the hypothesis drawn from the previous outbursts (see e.g. Mata Sánchez et al. 2017; Ravi 2017; Beri et al. 2019). We interpreted the sinusoidal drift of the X-ray pulsation as the result of the Doppler modulation of the pulsation frequency in a binary system with an orbital period of ~ 1 h. Phase-coherent timing analysis allowed us to refine the orbital ephemeris (Table 1).

Pulse phase delays estimated from the best-fitting timing solution show a clear jump of ~ 0.2 phase cycles. Similar shifts have been reported for SAX J1808.4–3658 (Burderi et al. 2006), XTE J1814–338 (Papitto et al. 2007), XTE J1807–294 (Riggio et al. 2008; Patruno et al. 2010), *SWIFT* J1749.4–2807 (Sanna et al. 2022), and MAXI J1816–195 (Bult et al. 2022, submitted). As shown in Fig. 2, the average pulse profile loses harmonic content after the phase jump, with an increase in the fractional amplitude of the fundamental component and a decrease of the third harmonic (detected at a 2σ c.l.). No correlation between the phase jump and X-ray count rate seems to exist. The origin of phase jumps in AMXPs is still an open question, and the investigation of the mechanisms proposed to explain them is beyond the scope of this work (see e.g. Bildsten 1998; Lamb et al. 2009; Poutanen, Ibragimov & Annala 2009; Riggio et al. 2011; Long, Romanova & Lamb 2012, for some of the proposed scenarios). Moreover, we found marginal evidence of modulation in the phase residuals with a ~ 2 d period and amplitude of ~ 0.03 phase cycles. If confirmed, this could signify a planet-like object (with mass $\lesssim 10^{-3} M_\odot$) gravitationally bound to the binary system.

We attempted to set a preliminary constraint on the NS dipolar magnetic field. Assuming the spin equilibrium for the X-ray pulsar, we can then express the magnetic field as:

$$B = 0.63 \zeta^{-7/6} \left(\frac{P_{\text{spin}}}{2 \text{ ms}} \right)^{7/6} \left(\frac{M}{1.4 M_\odot} \right)^{1/3} \times \left(\frac{\dot{M}}{10^{-10} M_\odot \text{ yr}^{-1}} \right)^{1/2} 10^8 \text{ G}, \quad (1)$$

where ζ (generally between 0.1 and 1) corresponds to the ratio between the magnetospheric radius and the Alfvén radius (see e.g. Ghosh & Lamb 1979; Wang 1996), P_{spin} and M are the pulsar spin period and mass, respectively, and \dot{M} represents the mass accretion rate on to the NS. Considering the peak unabsorbed flux (0.5–

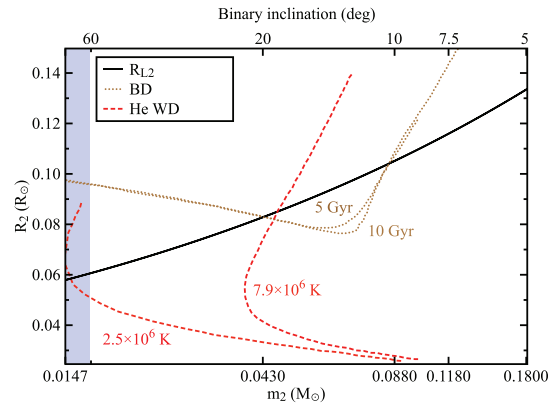


Figure 4. Radius–mass plane showing the size constraints on the Roche lobe-filling companion star MAXI J1957+032 (black solid line). The blue area defines the mass constraints for inclination angles between 60 and 90 deg. Red-dashed lines represent theoretical mass–radius relations for hot (7.9×10^6 K) and warm (2.5×10^6 K) Helium white dwarfs. Brown-dotted lines show low-mass main sequence/brown dwarfs of age 5 and 10 Gyr for solar metallicity abundances. The top axis indicates the corresponding binary inclination angle in degrees for a $1.4 M_\odot$ NS.

10 keV) and a source distance of 5 ± 2 kpc (Ravi 2017), we infer $\dot{M} \simeq 0.76 \times 10^{-10} M_\odot \text{ yr}^{-1}$ for an NS radius and mass of $1.4 M_\odot$ and 10 km, respectively. From equation (1), we estimate a dipolar magnetic field ranging between 1×10^8 G and 1.4×10^9 G, in line with the typical magnetic field of known AMXPs (see e.g. Mukherjee et al. 2015).

The NS mass function $f(m_2, m_1, i) \sim 1.6 \times 10^{-6} M_\odot$, combined with the absence of total eclipses or dips in the X-ray light curve (inclination $\lesssim 60^\circ$; see e.g. Frank, King & Lasota 1987), suggests a lower limit on the companion star mass of $m_2 \gtrsim 1.7 \times 10^{-2} M_\odot$ (for a $1.4 M_\odot$ NS), which increases up to $m_2 \gtrsim 2.1 \times 10^{-2} M_\odot$ if we consider a $2 M_\odot$ NS.

We derive the donor radius as a function of its mass, $R_2 \simeq 0.2 m_2^{1/3} P_{\text{orb},1\text{h}}^{2/3} R_\odot$, by combining the Roche Lobe overflow contact condition ($R_2 \approx R_{L2}$) with the NS mass function. To further investigate the nature of the donor star, in Fig. 4, we compare the latter expression (solid-black line) with different types of low-mass stars. Red-dashed lines represent theoretical mass–radius relations for warm (2.5×10^6 K) and hot (7.9×10^6 K) Helium white dwarfs (He WD; Deloye & Bildsten 2003). Warm He WDs seem unlikely given the required inclination $\sim 90^\circ$. On the other hand, hot He WDs would imply a donor mass $\sim 0.045 M_\odot$, with an orbital inclination of $\sim 20^\circ$. Brown-dotted lines represent numerically simulated mass–radius relations for brown dwarfs at 5 and 10 Gyr (Chabrier et al. 2009). Intersections between the curves suggest a brown dwarf donor star with mass of 0.043–0.085 M_\odot , which corresponds to an orbital inclination between 20 and 10 deg. However, we cannot exclude the possibility of the donor being bloated with respect to its thermal equilibrium radius because of irradiation from the compact object. Further studies are needed to favour one of the proposed scenarios. Nevertheless, these constraints on the donor mass strongly support the scenario for which the late-K/early M dwarf star identified as the optical counterpart of MAXI J1957+032 is not the donor star of the detected AMXP, but is instead a member of a triple system with an ultracompact AMXP binary (Ravi 2017).

Finally, the energy spectrum is well described by an absorbed soft black-body-like component ($kT \sim 0.4$ keV) compatible with emission from the NS surface plus a power-law-like component

characterized by $\Gamma \sim 1.6$ in line with typical thermal Comptonized components observed in the hard state of AMXPs (see e.g. Falanga et al. 2005; Gierliński & Poutanen 2005; Sanna et al. 2017a). The cooling of the black-body temperature and the increase of the power-law photon index as the source X-ray activity dims out are in line with the spectral evolution of the previous outbursts of the source (Beri et al. 2019), as well as other AMXPs (see e.g. Sanna et al. 2018c; Ng et al. 2021). We found no evidence for iron $K\alpha$, nor reflection components in the NICER band. Interestingly, a similar result has been reported for at least other four *ultracompact* AMXPs, i.e. IGR J16597–3704 (Sanna et al. 2018b), XTE J1807–294 (Campana et al. 2003), XTE J1751–305 (Miller et al. 2003), and *SWIFT* J1756.9–2508 (see e.g. Sanna et al. 2018a; Koliopanos et al. 2021). However, evidence for iron lines has been reported for compact systems such as NGC 6440 X–2 (Heinke et al. 2010), MAXI J0911–655 (Sanna et al. 2017b), and IGR J17062–6143 (Degenaar et al. 2017). Assuming a source distance $d = 5 \pm 2$ kpc (Ravi 2017), we constrain the peak luminosity during the latest outburst in the range $L = (3.2 - 17.2) \times 10^{35}$ erg s⁻¹ taking into account the distance uncertainty, consistent with MAXI J1957+032 being a very faint X-ray transient (see e.g. Wijnands et al. 2006; Beri et al. 2019).

ACKNOWLEDGEMENTS

PB acknowledges support from NASA through the NICER Guest Observer Program and the CRESST II cooperative agreement (80GSFC21M0002). NICER work at NRL is supported by NASA.

DATA AVAILABILITY

The data utilized in this article are publicly available at <https://heasarc.gsfc.nasa.gov/cgi-bin/W3Browse/w3browse.pl>, while the analysis products will be shared on reasonable request to the corresponding author.

REFERENCES

- Alpar M. A., Cheng A. F., Ruderman M. A., Shaham J., 1982, *Nature*, 300, 728
- Arnaud K. A., 1996, in Jacoby G. H., Barnes J., eds, ASP Conf. Ser. Vol. 101, *Astronomical Data Analysis Software and Systems V*. Astron. Soc. Pac., San Francisco, p. 17
- Baglio M. C., Russell D. M., Alabarta K., Saikia P., Lewis F., 2022, *Astron. Telegram*, 15448, 1
- Beri A., Altamirano D., Wijnands R., Degenaar N., Parikh A. S., Yamaoka K., 2019, *MNRAS*, 486, 1620
- Beri A., Altamirano D., Wijnands R., Degenaar N., Yamaoka K., 2022, *Astron. Telegram*, 15446, 1
- Bildsten L., 1998, *ApJ*, 501, L89
- Bult P. M. et al., 2022, *Astron. Telegram*, 15456, 1
- Burderi L., Di Salvo T., Menna M. T., Riggio A., Papitto A., 2006, *ApJ*, 653, L133
- Campana S., Rivasio M., Israel G. L., Mangano V., Belloni T., 2003, *ApJ*, 594, L39
- Chabrier G., Baraffe I., Leconte J., Gallardo J., Barman T., 2009, in Stempels E., ed., *American Institute of Physics Conference Series Vol. 1094*, 15th Cambridge Workshop on Cool Stars, Stellar Systems, and the Sun. p. 102
- Chakrabarty D., Jonker P. G., Markwardt C. B., 2016, *Astron. Telegram*, 9591, 1
- Chandra A. D., 2022, *Astron. Telegram*, 15460, 1
- Cherepashchuk A. M., Molkov S. V., Lutovinov A. A., Postnov K. A., 2015, *Astron. Telegram*, 7506, 1
- Degenaar N., Pinto C., Miller J. M., Wijnands R., Altamirano D., Paerels F., Fabian A. C., Chakrabarty D., 2017, *MNRAS*, 464, 398
- Deloye C. J., Bildsten L., 2003, *ApJ*, 598, 1217
- Di Salvo T., Sanna A., 2020, preprint ([arXiv:2010.09005](https://arxiv.org/abs/2010.09005))
- Falanga M. et al., 2005, *A&A*, 436, 647
- Frank J., King A. R., Lasota J. P., 1987, *A&A*, 178, 137
- Gendreau K. C. et al., 2016, in den Herder J.-W. A., Takahashi T., Bautz M., eds, *Proc. SPIE Conf. Ser. Vol. 9905, Space Telescopes and Instrumentation 2016: Ultraviolet to Gamma Ray*. SPIE, Bellingham, p. 99051H
- Ghosh P., Lamb F. K., 1979, *ApJ*, 232, 259
- Gierliński M., Poutanen J., 2005, *MNRAS*, 359, 1261
- Goodman J., Weare J., 2010, *Commun. Appl. Math. Comput. Sci.*, 5, 65
- Heinke C. O. et al., 2010, *ApJ*, 714, 894
- HI4PI Collaboration et al., 2016, *A&A*, 594, A116
- Koliopanos F., Vasilopoulos G., Guillot S., Webb N., 2021, *MNRAS*, 500, 5603
- Lamb F. K., Boutloukos S., Van Wassenhove S., Chamberlain R. T., Lo K. H., Clare A., Yu W., Miller M. C., 2009, *ApJ*, 706, 417
- Leahy D. A., 1987, *A&A*, 180, 275
- Long M., Romanova M. M., Lamb F. K., 2012, *New A*, 17, 232
- Mata Sánchez D., Charles P. A., Armas Padilla M., Buckley D. A. H., Israel G. L., Linares M., Muñoz-Darías T., 2017, *MNRAS*, 468, 564
- Miller J. M. et al., 2003, *ApJ*, 583, L99
- Mukherjee D., Bult P., van der Klis M., Bhattacharya D., 2015, *MNRAS*, 452, 3994
- Negoro H. et al., 2015, *Astron. Telegram*, 7504, 1
- Negoro H. et al., 2022, *Astron. Telegram*, 15440, 1
- Ng M. et al., 2021, *ApJ*, 908, L15
- Ng M. et al., 2022, *Astron. Telegram*, 15444, 1
- Papitto A., di Salvo T., Burderi L., Menna M. T., Lavagetto G., Riggio A., 2007, *MNRAS*, 375, 971
- Patruno A., Hartman J. M., Wijnands R., Chakrabarty D., van der Klis M., 2010, *ApJ*, 717, 1253
- Patruno A., Watts A. L., 2021, *Astrophys. Space Sci. Libr.*, 461, 143
- Poutanen J., Ibragimov A., Annala M., 2009, *ApJ*, 706, L129
- Ravi V., 2017, *ApJ*, 851, 114
- Remillard R. A. et al., 2022, *AJ*, 163, 130
- Riggio A., Di Salvo T., Burderi L., Menna M. T., Papitto A., Iaria R., Lavagetto G., 2008, *ApJ*, 678, 1273
- Riggio A. et al., 2011, in AIP Conf. Proc. Vol. 1357, *Radio Pulsars: An Astrophysical Key to Unlock the Secrets of the Universe*. Am. Inst. Phys., New York, p. 151
- Sanna A. et al., 2016, *MNRAS*, 459, 1340
- Sanna A. et al., 2017a, *MNRAS*, 466, 2910
- Sanna A. et al., 2017b, *A&A*, 598, A34
- Sanna A. et al., 2018a, *MNRAS*, 481, 1658
- Sanna A. et al., 2018b, *A&A*, 610, L2
- Sanna A. et al., 2018c, *A&A*, 617, L8
- Sanna A. et al., 2022, *MNRAS*, 514, 4385
- Sugimoto J. et al., 2015, *Astron. Telegram*, 8143, 1
- Tanaka K. et al., 2016, *Astron. Telegram*, 8529, 1
- van den Eijnden J., Fender R., Woudt P., Miller-Jones J., Motta S., 2022, *Astron. Telegram*, 15462, 1
- Verner D. A., Ferland G. J., Korista K. T., Yakovlev D. G., 1996, *ApJ*, 465, 487
- Wang Y.-M., 1996, *ApJ*, 465, L111
- Wang Y., Bellm E. C., Jaodand A., 2022, *Astron. Telegram*, 15455, 1
- Wijnands R. et al., 2006, *A&A*, 449, 1117
- Wilms J., Allen A., McCray R., 2000, *ApJ*, 542, 914

This paper has been typeset from a $\text{\TeX}/\text{\LaTeX}$ file prepared by the author.